

Dark matter annihilation in the halo of the Milky Way

Felix Stoehr¹, Simon D. M. White¹, Volker Springel¹,
Giuseppe Tormen² and Naoki Yoshida³

¹Max-Planck-Institut für Astrophysik, Karl-Schwarzschild-Str. 1, 85748 Garching bei München, Germany

²Dipartimento di Astronomia, Università di Padova, vicolo dell'Osservatorio 5, 35122 Padova, Italy

³National Astronomical Observatory Japan, Mitaka, Tokyo 181-8588, Japan

Email: felix@mpa-garching.mpg.de, swhite@mpa-garching.mpg.de, volker@mpa-garching.mpg.de, tormen@pd.astro.it, naoki@th.nao.ac.jp

Accepted 2003 July 29. Received 2003 July 7

ABSTRACT

If the dark matter in the Universe is made of weakly self-interacting particles, they may self-annihilate and emit γ -rays. We use high resolution numerical simulations to estimate directly the annihilation flux from the central regions of the Milky Way and from dark matter sub-structures in its halo. Although such estimates remain uncertain because of their strong dependence on the structure of the densest regions, our numerical experiments suggest that less direct calculations have overestimated the emission both from the centre and from halo sub-structure. We estimate a maximal enhancement of at most a factor of a few with respect to a smooth spherical halo of standard Navarro-Frenk-White (NFW) structure. We discuss detection strategies for the next generation of γ -ray detectors and find that the annihilation flux may be detectable, regardless of uncertainties about the densest regions, for the annihilation cross-sections predicted by currently popular elementary particle models for the dark matter.

Key words: methods: N -body simulations – Galaxy: halo – dark matter.

1 INTRODUCTION

The nature of the dark matter (DM) in the Universe is one of the most prominent unsolved questions in cosmology. Among the best motivated candidates for DM is a weakly interacting massive particle (WIMP) in the mass range 10 to 10^4 GeV c^{-2} . In minimal supersymmetric extensions of the standard model of particle physics, a stable, neutral particle with these properties (usually called a neutralino) arises naturally as the lightest supersymmetric particle.

In recent years, a growing effort has been dedicated to detecting WIMPs directly through the energy deposited by elastic WIMP-nucleon scattering in massive, cryogenically cooled bolometers. A different detection strategy is possible if WIMPs are Majorana particles. In this case, pair-annihilations can occur, producing high-energy neutrinos, positrons, antiprotons and γ -rays. The resulting γ -ray fluxes might be detectable with current- or next-generation telescopes. So far neither technique has detected a DM particle.

Both ground-based air-shower-Čerenkov telescopes (ACT) and space-borne telescopes might be able to detect annihilation γ -rays. Such observations can be used to constrain WIMP parameters – in particular, the self-annihilation cross-section and the particle mass. Predictions of the expected flux require not only these parameters but also a detailed knowledge of the structure of regions of high DM density, i.e. of DM haloes. This is because the annihilation flux (in photons $\text{cm}^{-2} \text{s}^{-1}$) may be written as:

$$F = \frac{N_\gamma \langle \sigma v \rangle}{2 m_{DM}^2} \int_V \frac{\rho_{DM}^2(\mathbf{x})}{4\pi d^2(\mathbf{x})} d^3x, \quad (1)$$

where N_γ is the number of photons produced per annihilation, $\langle \sigma v \rangle$ is the averaged product of cross-section and relative velocity, ρ_{DM} is the DM density, V is the halo volume, m_{DM} is the mass of the DM particle and d the distance from each point in the halo to the observer. The density squared weighting of the integrand in this equation results in most of the flux in dark DM haloes being produced by the small fraction of their mass in the densest regions.

Two specific regions have been suggested as dominating the annihilation signal from haloes. A large contribution could come from the innermost part of the halo. For a distant spherically symmetric system equation (1) becomes

$$F = \frac{N_\gamma \langle \sigma v \rangle}{2 d^2 m_{DM}^2} \int_0^{r_{200}} \rho_{DM}^2(r) r^2 dr, \quad (2)$$

so if the inner density profile is $\propto r^{-1.5}$ or steeper, the emitted flux diverges at the centre. A lower cut-off must then be specified on physical grounds, for example at the point where the annihilation timescale for the DM becomes equal to the lifetime of the halo. This divergent case might, perhaps, be relevant, since at least some high resolution numerical simulations have suggested that the inner cusps of DM haloes could be this steep (Moore et al. 1999; Calcanéo-Roldán & Moore 2000). Both the data we present below and the study of Power et al. (2003) suggest, however, that cold dark matter (CDM) haloes are substantially less concentrated than this.

A second contribution can come from small-scale structure in the DM distribution in the halo. It is now well established that

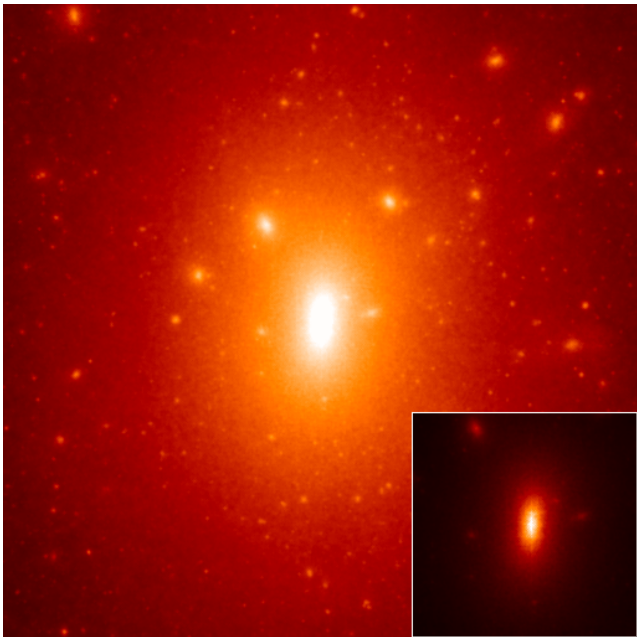


Figure 1. The distribution of DM in our highest-resolution simulation GA3n. The region displayed is a cube of side 270 kpc, i.e. 1 times r_{200} . Each particle is weighted by its local density so that the picture represents an image in annihilation radiation. The main image has a logarithmic intensity scale, whereas the small image reproduces the centre on a linear intensity scale.

5 to 10 per cent of the halo mass in (CDM) haloes is contained in gravitationally self-bound substructures (Moore et al. 1999; Klypin et al. 1999). If the central regions of these subhaloes were dense enough, they could produce a substantial fraction of the total annihilation radiation from the halo (Calcanéo-Roldán & Moore 2000).

In recent years, advances in integrator software, multi-mass initial condition techniques and computer speed have made it possible to simulate the DM halo of the Milky Way with sufficient resolution to see the dense regions which dominate the annihilation signal. In the present paper we use a series of high resolution N-body DM simulations to predict the annihilation flux from a CDM halo similar in mass to the halo of the Milky Way.

In the next section we briefly describe the N-body simulations we have carried out. In Section 3 we measure circular velocity profiles for our haloes and discuss their implications for the strength of the annihilation flux from the inner Galaxy. In Section 4 we then analyse the flux enhancements due to bound substructures and to other density irregularities. In Section 5, we use the annihilation cross-sections currently considered plausible to evaluate whether halo γ -ray production is likely to be detectable with the next generation of telescopes. Finally, Section 6 summarises our results and compares them to those of other workers.

2 N-BODY SIMULATIONS

In this paper we use simulations of the ‘Milky Way’ halo studied previously by Stoehr et al. (2002; hereafter SWTS). We work with a flat Λ -dominated CDM universe, with matter density $\Omega_m = 0.3$, cosmological constant $\Omega_\Lambda = 0.7$, expansion rate $H_0 = 70 \text{ km s}^{-1} \text{ Mpc}^{-1}$, index of the initial fluctuation power spectrum $n = 1$, and present-day fluctuation amplitude $\sigma_8 = 0.9$. We begin

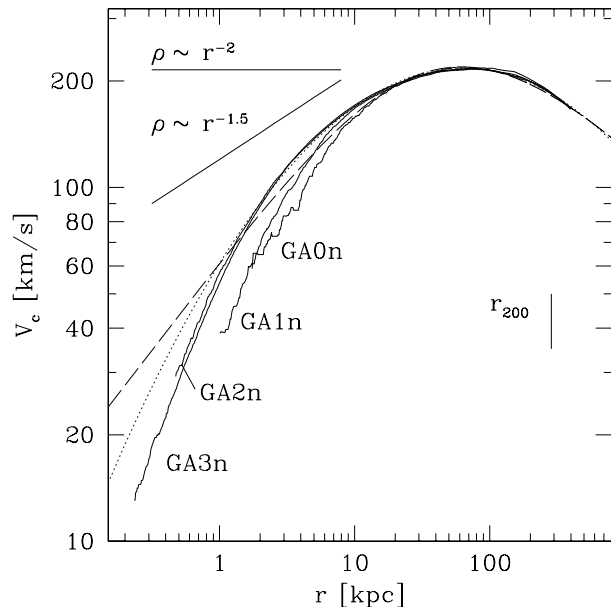


Figure 2. Circular velocity curves for the simulations GA0n, GA1n, GA2n and GA3n. The vertical line indicates the location of the virial radius r_{200} . The best-fitting NFW profile with concentration $c_{NFW} = 10$ is plotted in long dashes. A fit of the form proposed by SWTS with $a=0.17$ is shown in dots. At small radii the slope for GA3n is considerably below that corresponding to a density profile with $\rho \propto r^{-1.5}$.

with an intermediate resolution dark matter simulation of a ‘typical’ region of the Universe ($N \sim 6 \times 10^7$, particle mass $\sim 10^8 M_\odot$) for which the techniques of Springel et al. (2001a; hereafter SWTK) have been used to follow the formation of the galaxy population. We identify a relatively isolated ‘Milky Way-like’ galaxy which had its last major merger at $z > 1.5$. Then we resimulate its halo at a series of higher resolutions, again using techniques from Tormen et al. (1997) and SWTK and the N-body code GADGET¹ (Springel et al. 2001b). We have rerun the simulations of SWTS with higher force accuracy and have added an additional simulation with even higher mass resolution. In the simulations GA0n, GA1n, GA2n and GA3n the resimulated halo has 14 097, 128 276, 1204 411 and 10 089 396 particles, respectively within r_{200} , the radius within which the enclosed mean density is 200 times the critical value.

The simulated haloes were scaled-down in velocity, mass and radius (but with unchanged density and time-scales) so that their circular velocity peaks at 220 km s^{-1} . With this scaling, dark matter particle masses are 1.8×10^8 , 1.9×10^7 , 2.0×10^6 and $2.5 \times 10^5 M_\odot$ and Plummer equivalent softening lengths are 1.8, 1.0, 0.48 and 0.24 kpc in GA0n, GA1n, GA2n and GA3n, respectively. In all four $r_{200} \approx 270 \text{ kpc}$. Note that since the stars of the Milky Way contribute significantly to its measured rotation velocity, our chosen scaling probably produces too large a mass for the Milky Way’s halo and thus also for substructures within it. We use SUBFIND (SWTK) to identify self-bound substructure. A more detailed description of the simulation set-up can be found in SWTS. Fig. 1 shows the projected, density-weighted DM distribution in a logarithmic representation which corresponds to an image of its annihilation radiation. Many substructures are visible. A representation of

¹ www.mpa-garching.mpg.de/gadget/

the halo centre with a linear intensity scale (but on the same angular scale) is shown in the inset.

3 SMOOTH HALO STRUCTURE

The most crucial parameter determining the annihilation rate in a smooth halo is the point at which the slope of its density profile passes through the critical value -1.5 . Most of the annihilation radiation will come from this region. It is difficult to distinguish slopes in logarithmic plots of density against radius, so in Fig. 2 we show circular velocity profiles

$$V_c(r) = \left[\frac{GM(<r)}{r} \right]^{1/2} = \left[\frac{G}{r} \int_{V(r)} \rho_{DM}(\mathbf{x}) dV \right]^{1/2}, \quad (3)$$

where $V(r)$ is the region within distance r of halo centre. We plot these curves down to a distance from the centre equal to the softening length, and we overplot the best-fitting Navarro-Frenk-White (NFW) profile (Navarro et al. 1997) in dashes. We also indicate the critical value for the slope, $\rho(r) \propto r^{-1.5}$, and the value for an isothermal profile $\rho(r) \propto r^{-2}$. We find the NFW profile

$$\rho(r) = \frac{3H_0^2}{8\pi G} \frac{\delta_c}{c_{NFW} x (1 + c_{NFW} x)^2} \quad (4)$$

with $x = r/r_{200}$ and $c = 10$ to be a reasonably good fit to our data outside the inner core region. A better fit is a parabolic function of the form proposed by SWTS with a width parameter of $a=0.17$ (the dotted curve in the figure). This profile has a substantially shallower density profile at small radii than the NFW profile. The measured circular velocity profiles of GA2n and GA3n agree very well, but a comparison with GA1n and GA0n suggests that this apparent convergence is in part a fluke. The curves for the two lower-resolution simulations converge to within 5 per cent of the high-resolution answer beyond about 5 times their respective softening lengths. Assuming this to be true for GA2n and GA3n also, the inner slope of the density profile of our simulated halo is established to be well below -1.5 . With this criterion, convergence for GA3n is achieved just outside 1 kpc or at about 0.4 per cent of r_{200} . This agrees with the expectation from the convergence study of Power et al. (2003) who performed a large number of simulations of several haloes using two different N-body codes as well as a wide variety of code parameters (timestep, softening, particle number, etc.).

The concentration parameter for our NFW fit to our halo is $c_{NFW} = 10$. Thus, $\delta_c = 4.48 \times 10^4$ and the above value of r_{200} implies a scale radius $r_s = 27$ kpc, and a density at the Sun's position ($r_0=8.0$ kpc) of $\rho_0 = 1.2 \times 10^7 M_\odot/\text{kpc}^3 = 0.46 \text{ GeV } c^{-2} \text{ cm}^{-3}$.

For our NFW fit, half of the annihilation radiation is predicted to come from within $0.26 r_s$ which is 7 kpc. Thus the resolution in GA3n appears easily sufficient to measure the bulk of the emission, even though still better resolution would clearly be desirable. Unfortunately, the numerical situation will not improve dramatically in the next few years unless revolutionary new techniques are discovered. As discussed at length by Power et al. (2003), an increase in halo particle number by (say) two orders of magnitude would provide an increase in length resolution at halo centre by at best a factor of 10.

Many authors have tried to determine the inner slope of dark halo density profiles through physically based analytic arguments (Peebles 1980; Hernquist 1990; Syer & White 1998;

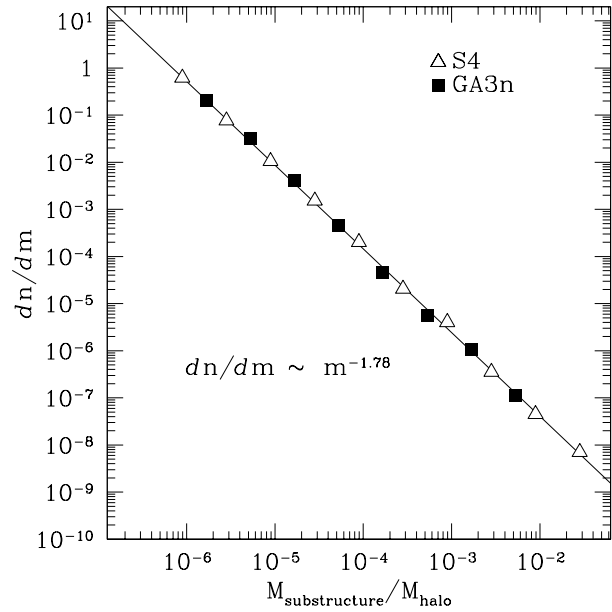


Figure 3. Subhalo mass functions for the GA3n (Milky Way) and S4 (cluster) simulations. Subhaloes identified by SUBFIND and with ten or more particles are included in these distributions.

Nusser & Sheth 1999; Subramanian et al. 2000; Dekel et al. 2002) but despite some interesting ideas a convincing final answer is still missing. For the purposes of this paper the critical issue is whether the slope of the density profile interior to the points for which it has so far been estimated accurately from simulations (i.e. at radii below 1 kpc) remains significantly shallower than -1.5 . If it does, then the integral over the smooth halo density distribution is convergent and can be estimated reasonably accurately from high resolution simulations, for example from GA3n which is currently the best resolved simulation of a galaxy halo ever carried out.

Bergström, Ullio & Buckley (1998) show that if a smooth NFW halo, similar to that of Fig. 2, is a good description of the Milky halo of the Way, then for some minimal supersymmetric extensions of the Standard Model (MSSM) the γ -ray flux may just be detectable with next generation telescopes. The flux could, however, be significantly enhanced if the density distribution within the halo is sufficiently clumpy (Bergström et al. 1999; Calcanéo-Roldán & Moore 2000; Taylor & Silk 2003). We now estimate whether the clumpiness of our simulated haloes is enough to produce a large enhancement.

4 HALO SUBSTRUCTURE

In GA0n, GA1n, GA2n and GA3n the total mass in gravitationally bound substructures, identified with SUBFIND, is 1.7, 3.0, 5.1 and 4.1 per cent, respectively; the fluctuations are due to the exclusion or inclusion of one or two massive satellites within the radius r_{200} that we consider to define the halo boundary. These percentages are very similar to those found in the cluster simulations of SWTK. In Fig. 3 we show the abundance of substructures as a function of mass fraction for our highest resolution simulation GA3n, as well as for S4, the highest-resolution simulation of SWTK.

These two mass functions are remarkably similar and are very close to a power-law $dn/dm \propto m^{-1.78}$ as shown by the solid

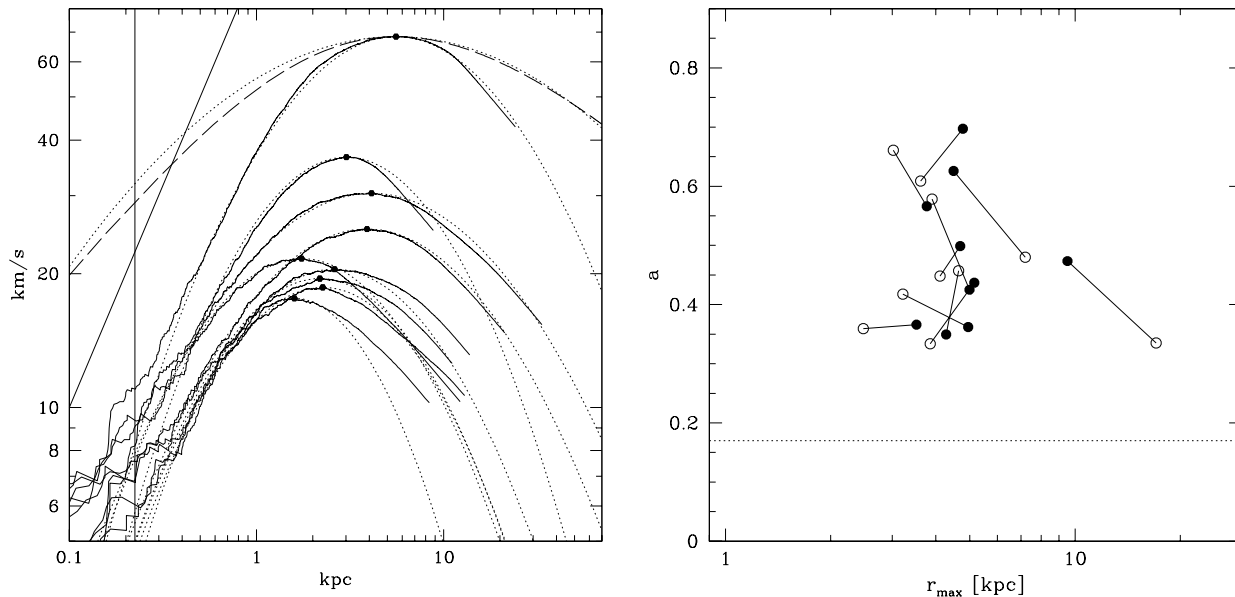


Figure 4. *Left-hand panel:* Circular velocity curves for the GA3n subhaloes ranked 1, 5, 10,...40 in mass (solid) together with corresponding SWTS fits (dotted). For comparison an NFW profile (dashed) and an SWTS profile with $a = 0.17$ (the value for the main halo) are overlotted on the most massive subhalo. The vertical solid line shows the softening length, the diagonal line the profile slope corresponding to a constant density. *Right-hand panel:* Values of a and r_{max} (the radius of maximum circular velocity) for matching subhaloes in GA2n (open) and GA3n (filled). The horizontal line is $a = 0.17$, the value for the main halo.

line in the figure. They are consistent with the findings of other authors (Moore et al. 1999; Klypin et al. 1999; Metcalf & Madau 2001; Font et al. 2001; Helmi et al. 2002), although the range of published values (1.75 to 1.9) suggests that the close agreement between these two particular haloes is likely to be a fluke. Some variation is undoubtedly due to the fact that different authors use different algorithms to define substructure, but these effects have not yet been studied in detail. Note that such slopes are also found at low mass for the mass function of isolated haloes in a Λ CDM Universe, suggesting that the fraction of mass lost depends only weakly on the initial mass of an accreted DM halo. These slopes are shallow enough to ensure that most of the mass in substructures is contained in the few most massive objects. Thus we do not expect the total mass in substructure to increase significantly as resolution is extended below our current limit.

As suggested by Bergström et al. (1999) and Calcanéo-Roldán & Moore (2000), if these subhaloes are sufficiently concentrated, they can make a substantial contribution to the total annihilation flux from the halo. Just as for the main halo, the critical question regards the structure in their inner regions – in particular, whether they contain more or less mass at the highest densities than does the core of the main halo. Recently Hayashi et al. (2003) carried out high-resolution simulations of the tidal stripping of satellites to assess how their internal structure is affected by the removal of the outer material. Their results show clearly that the stripping process reduces the density of an accreted object at *all* radii, not just in its outer regions. Thus tidal effects progressively lower the annihilation luminosity of an accreted system. If its γ -ray flux was convergent in the inner regions while it was an independent system, then it converges even more rapidly once it has become a partially stripped ‘satellite’. Both the individual satellite simulations of Hayashi et al. (2003) and the results plotted in SWTS, suggest that the inner structure of

halo substructures corresponds to density profiles *shallower* than NFW.

We study this point in more detail in the left-hand panel of Fig. 4 which shows the circular velocity profiles for a set of representative subhaloes in GA3n. This can be compared with Fig. 2 of SWTS which gives a similar plot for the 9 times lower resolution simulation GA2 except that we here take only gravitationally bound particles into account. Clearly, the parabolic fitting formula suggested by SWTS provides an excellent characterisation of circular velocity curves in this higher resolution case also. As before, the circular velocity curves for the subhaloes have substantially narrower peaks than the curve for the main halo. Indeed, the values of the width parameter a for GA3n subhaloes are very similar to those for GA2 subhaloes. The shape convergence for subhalo density profiles is demonstrated in the right-hand panel of Fig. 4. We identify corresponding subhaloes (i.e. subhaloes which formed from the infall of the same progenitor object onto the main halo) in GA2n and GA3n. Then we plot a (a, r_{max}) point for each of the two simulations and join the symbols by a line. The agreement of the values found is quite good and there is no systematic trend in either parameter as the mass resolution is increased by an order of magnitude. The results of Hayashi et al. (2003) confirm that subhalo centres are significantly *less* cuspy either than the objects from which they formed or than isolated haloes of similar mass. Their subhalo circular velocity curves are very well fit by our parabolic formula and require similar values of a . This agreement for two different simulation techniques and over a resolution range of an order of magnitude suggests that the reduced concentration of simulated satellites is unlikely to be an effect of numerical relaxation, but more likely reflects the influence of tidal shocking on the inner regions of satellite subhaloes.

We now proceed to estimate the annihilation luminosity of our simulations directly in order to evaluate how much of the flux is

contributed by the various different parts of the system. To do this we evaluate the ‘astrophysical’ part of equation (1) in the form

$$J = \int_V \rho_{DM}^2 dV = \sum_{i=1}^{N_{200}} \rho_i m_i, \quad (5)$$

where ρ_i is an estimate of the DM density at the position of the i th particle, m_i is its mass, and N_{200} is the total number of particles within r_{200} . With this representation of the flux it is easy to evaluate the contribution from any sub-element of the halo simply by restricting the sum to the relevant particles. We will consider how these J s should be converted into γ -ray detectability limits for various WIMP parameters in Section 5.

The quality of our estimate of J will obviously depend strongly on the quality of our estimates of DM density. For a given simulation we would like these estimates to have the maximum possible resolution. We have elected to determine the ρ_i by Voronoi-tessellation. This procedure uniquely divides three dimensional space into convex polyhedral cells, one centred on each particle. A cell is defined to contain all points closer to its particle than to any other. The density estimate for each particle is then its mass divided by the volume of its cell. We have used the publicly available package QHULL² to make these estimates. One major advantage of this scheme in comparison, say, to density estimation with an SPH kernel is that it is parameter-free and has very high resolution; the density estimate for each particle is determined by the position of its few nearest neighbours. Another is that it is unbiased and that the sum $\sum_i^{N_{200}} m_i/\rho_i$ recovers the full volume.

A direct numerical evaluation of J using equation 5 will differ from the value obtained by carrying out the appropriate integral over the circular velocity curves of Fig. 2. This is because any deviation from strict spherical symmetry results in the sum of $\rho_i m_i$ over a spherical shell being larger than the product of its total mass and its mean density. Thus flux ‘enhancements’ will result from bound subhaloes, from unbound streams, from the overall flattening of the halo and from noise in the density estimates due to discreteness effects. The last contribution is easily estimated. In any region where the mean particle separation is small compared to the length-scale for density variations, our Voronoi scheme will give 22 per cent more flux than would be obtained using the average density. For an ellipsoidal NFW halo with axial ratios 1:1.2:1.8, similar to what we measure in the inner regions of our simulated haloes, the enhancement due to the flattening is about 15 per cent. The enhancement due to bound structures is estimated explicitly below.

If subhaloes were simply scaled down copies of the main halo with $r \propto M^{1/3}$, then their fractional contribution to the annihilation luminosity would be the same as their fractional contribution to the mass, i.e. roughly 5 per cent. However, the algorithm SUBFIND bounds substructures at the point where their density equals the local density of material within the main halo. As a result, the internal structure of a subhalo cannot be similar to the main halo as a whole, but might be similar to that part of it which lies interior to the position of the subhalo (scaled down in size by the cube root of the ratio of the substructure’s mass to the total halo mass within a sphere passing through it). If such self-similarity were actually to hold then the annihilation luminosity per unit mass (i.e. the quantity J/M) would be the same for the subhalo as for the main halo interior to its position. In fact, however, the study of Hayashi et al. (2003) shows that the density of a satellite at radii approaching its

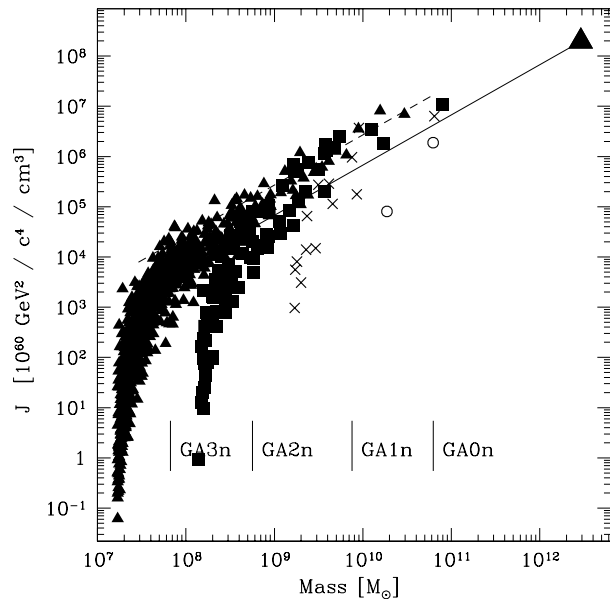


Figure 5. The sum J , which is proportional to the expected annihilation luminosity, is plotted as a function of subhalo mass for all subhaloes with more than 50 particles in GA0n (circles), GA1n (crosses), GA2n (dots) and GA3n (triangles). The value of J for the main halo as a whole is indicated by the larger triangle. Subhaloes with the same J/M as the GA3n main halo would lie on the solid line. The dashed line corresponds to a 4 times larger value of J/M . Vertical lines indicate subhalo masses corresponding to 200 particles in each of the four simulations. Above these limits subhaloes in all four simulations have similar values of J/M with no obvious trend with subhalo mass.

tidal limit is reduced by a substantially greater factor than that in the regions near the peak of its circular velocity curve. This effect increases the luminosity per unit mass of a substructure relative to the main halo interior to its position. Higher values might also be expected because subhaloes had lower mass progenitors at high redshift than did the main halo, and so began life with higher concentration (see Navarro et al. (1997) and Bullock et al. (2001) for estimates). On the other hand, we have argued above that tidal effects also reduce the concentration of the inner core of subhaloes, thus reducing their annihilation luminosities. The J/M values for substructures reflect the combination of all these effects.

Fig. 5 shows the sums J – which are proportional to annihilation luminosity – as a function of subhalo mass for all four of our simulations and for subhaloes containing at least 50 particles. A point is also plotted for the main halo as a whole. If subhaloes were similar to the main halo as a whole, they would lie along the solid line of constant J/M . Clearly, J/M is larger for the subhaloes. Vertical lines in the plot indicate subhalo masses corresponding to 200 particles for each of the four simulations. Above these limits the values of J for subhaloes in GA0n, GA1n and GA2n appear to converge approximately to those found in GA3n. This suggests that the GA3n results may also be reliable for subhaloes with more than 200 particles. Such GA3n subhaloes have J/M values typically 4 times larger than the main halo as a whole and twice as large as the part of the main halo interior to their position. The other effects discussed above presumably account for the remaining factor. Note that there is no indication that J/M depends on subhalo mass for subhaloes with more than 200 particles. This implies that the total luminosity

² www.geom.umn.edu/software/qhull/

from subhaloes, like the total subhalo mass, is dominated by the largest objects.

The left-hand panel of Fig. 6 shows the contributions of different components to the total estimated annihilation luminosity of our simulated haloes. The smooth halo component is shown by a dashed line. This was calculated from the circular velocity curves of Fig. 2 and was corrected up by 15 per cent to account for the fact that the main halo is ellipsoidal rather than spherical, and by 22 per cent to account for discreteness noise in our Voronoi density estimates. The total luminosity from bound subhaloes is indicated by a dotted line. The remainder of the total halo luminosity is then assumed to come from unbound substructure and is indicated by a dot-dashed line. All values are given in units of the corresponding smooth halo luminosities. The values of the latter, relative to GA3n, are indicated by boxes in the figure. The close agreement of the circular velocity curves for GA3n and GA2n results in identical predictions for the smooth halo luminosity. The values predicted for GA1n and GA0n are only smaller by 20 and 35 per cent respectively, suggesting that convergence is approximately achieved in the inner regions even for relatively low mass resolution. The reason is simply that the simulations predict the half-light radii of haloes to be relatively large (8.6 kpc in GA3n) in comparison with the nominal resolution.

In GA3n, the total luminosity is a factor of 1.7 – the ‘clumpiness factor’ – times the value for a smooth spherical halo with the same circular velocity curve. Of this 70 per cent increase, 25 per cent is due to bound substructures with 10 or more particles, 22 per cent to Poisson discreteness noise, 15 per cent to the flattening of equidensity surfaces in the inner halo and 8 per cent to unbound fluctuations. Although the fraction of the annihilation luminosity contributed by substructure is very similar in GA2n and GA3n, it is clear that this does not indicate absolute convergence. The total mass in substructures in GA2n is 1.2 times larger than in GA3n (a consequence of the chance inclusion of a couple of substructures in GA2n which lie just outside r_{200} in GA3n). On the other hand, the luminosity per unit mass of substructures is a factor of 1.11 larger in GA3n than in GA2n. In addition, the luminosity of the inner 10 per cent of r_{200} (which dominates the luminosity of the smooth halo) is 5 per cent larger in GA3n than in GA2n.

In order to get an idea of an upper limit of the additional luminosity which might be found at higher resolution it is instructive to extrapolate the variation between GA1n and GA2n down to a mass resolution of one solar mass. (Note that GA3n lies well *below* this extrapolation.) Even at such high resolution, the total luminosity is predicted to be only about 3.0 times that of the smooth halo in GA3n.

Lake (1990) and Bergström et al. (1999) suggested that if a dark matter substructure happens to be close to the observer, it might be more easily detected than the Galactic Centre itself. This possibility was judged plausible by Tasitsiomi & Olinto (2002; hereafter TO) who assumed subhaloes to be distributed through the Galactic halo like the DM itself and tried various models for their internal structure. For the internal structure predicted by our simulations, however, it is very unlikely that any substructure will outshine the Galactic Centre. The most massive and most luminous substructures are rare and tend to avoid the inner Galaxy. They presumably correspond to the known satellites of the Milky Way (see SWTS), the nearest of which is Sagittarius, 24 kpc from the Sun. The greater abundance predicted for less massive substructures is insufficient to compensate for their lower predicted luminosities – the chance that the received flux is dominated by an unexpectedly nearby low-mass substructure is predicted to be very low.

These issues are clarified in the right-hand panel of Fig. 6, where we plot cumulative radial distributions for total mass and total annihilation luminosity *exclusive of substructure*, as well as for the number, mass and annihilation luminosity of subhaloes. While the diffuse luminosity is much more strongly concentrated towards the Galactic Centre than the mass, all properties of the substructure are more *weakly* concentrated. In addition, since J/M is independent of subhalo mass, which in turn is almost independent of distance from the Galactic Centre, the distributions of substructure number, mass and luminosity are all rather similar. The latter two are much noisier than the first because most of the mass and most of the luminosity come from the few most massive subhaloes. At 8 kpc, the Sun’s galactocentric radius lies in the region where most of the diffuse annihilation radiation originates, but well inside any of the resolved subhaloes in GA3n (the first is at $R = 17.2$ kpc) and even further inside any of the more massive subhaloes (the first is at $R = 70$ kpc).

Whereas Fig. 6 was constructed directly from GA3n, based on our Voronoi estimate of J/M for each particle, we obtain almost identical results if we instead use our SWTS model fits to main halo and subhalo circular velocity curves and assume that J/M is 4 times the value for the main halo for all subhaloes which are too small for circular velocity curves to be estimated. Again, this suggests that GA3n has high enough resolution to get reliable results for the problem at hand.

5 DETECTABILITY

For our highest resolution simulation GA3n we can make artificial sky maps of the annihilation radiation by choosing appropriate positions for the Sun within the model. Fig. 7 shows the result of this exercise based on six possible solar positions. Even though we average the predicted surface brightness around circles of fixed Galactocentric angle, there is significant variation among the resulting profiles. This is primarily a consequence of the prolate structure of the inner regions, clearly visible in Fig. 1. The profiles flatten out within about 10° , quite possibly as a consequence of poor numerical resolution. *Prima facie* this seems plausible since the angular scale corresponding to our softening length (the vertical lines in the plots) is only 4 or 5 times smaller than the radius where the profiles bend. Some indication of the strength of this effect is given by the two curves. These indicate predictions based on SWTS (solid) and NFW (dashed) fits to the circular velocity profile of GA3n, corrected up by a clumpiness factor of 1.7. Both inward extrapolations predict substantially more flux within a few degrees than the direct numerical estimates.

It is important to note, however, that the area potentially available for a measurement at distance θ from the Galactic Centre increases as θ (for $\theta \ll \pi/2$). As a result, the counts available to detect a signal vary as θ^2 times the profiles shown in the left panel of Fig. 7 while, for a uniform background, the noise against which the signal must be detected grows only as θ . Thus the potential signal-to-noise for a detection, shown in the right-hand panel, is given by θ times the profile. This function is quite flat out to 20° , both for the directly measured profiles and for our two alternative fitting formulae. This has two consequences: (i) since for many observations the background is higher in the direction of the Galactic Centre, it may be advantageous to observe at large θ if one has a detector with sufficient field of view; and (ii) the estimates of detectability which we give below for detectors with a wide field of view are not greatly affected by the resolution of our simulation.

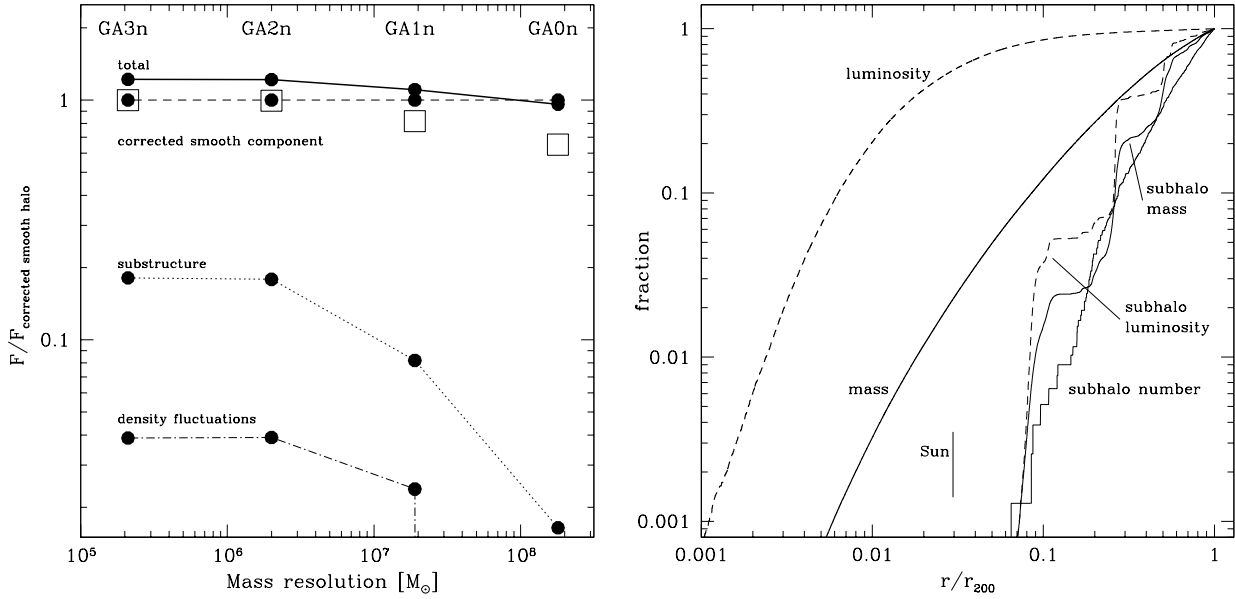


Figure 6. *Left-hand panel:* The luminosities of different halo components as a function of mass resolution. The values for each simulation are scaled so that the luminosity of its smooth halo is unity after correction for Poisson discreteness and flattening. The large squares show the luminosities of these smooth halo components in units of the value found in GA3n. *Right-hand panel:* Cumulative luminosity (dashed) and mass (solid) for the GA3n main halo (thick) and for the subhaloes with more than 50 particles (thin) as a function of radius.

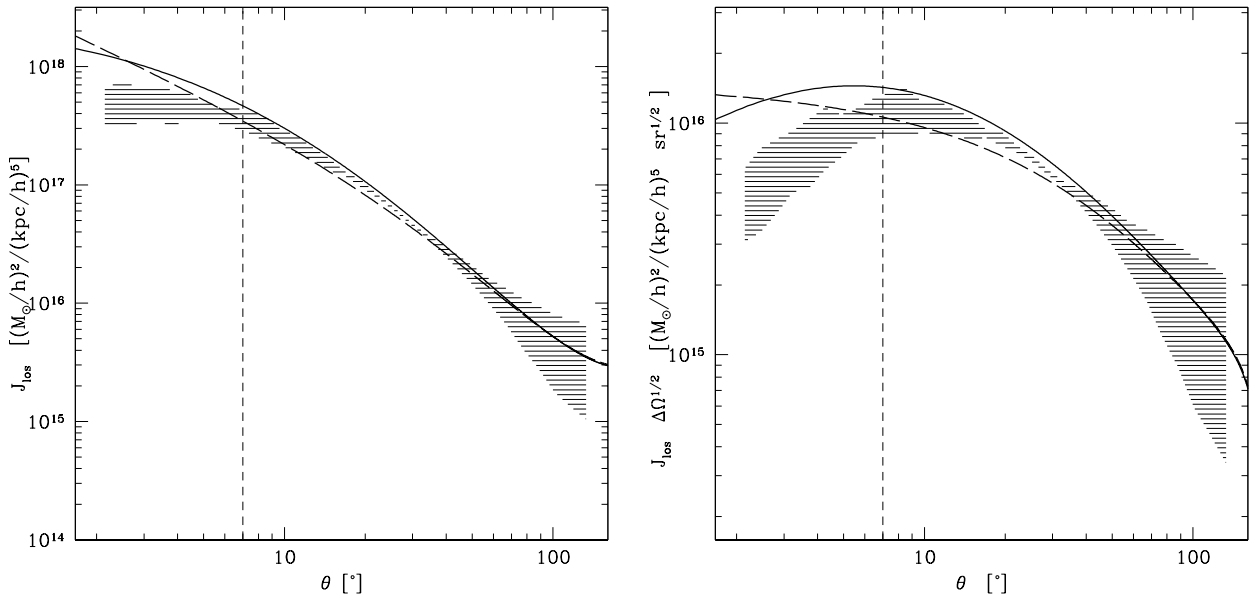


Figure 7. Mean predicted surface brightness of annihilation radiation as a function of angular distance from the Galactic Centre. The hatched regions enclose profiles estimated directly from six different ‘solar’ positions 8kpc from the centre of GA3n, while the two curves gives results based on SWTS (solid) and NFW (dashed) fits to the circular velocity curve, together with an enhancement factor of 1.7. In the left-hand panel the surface brightness profiles are plotted directly, whereas on the right they are multiplied by one power of the angle θ to represent the signal-to-noise expected in an observation of fixed duration of a region whose size increases in proportion to θ , (specifically $[\theta, 1.01\theta]$). Vertical dashed lines indicate the angle subtended by the gravitational softening length at the distance of the Galactic Centre.

Using these results, we can check if the inner regions of the Milky Way or a substructure halo close to the Sun might be detectable with next generation γ -ray telescopes. We use the excellent package DARKSUSY³ to compute the cross-sections $\langle\sigma v\rangle$ and neutralino masses m_χ for a Monte Carlo sampling of the MSSM parameter space. The results are shown in Fig. 8. From roughly two million models randomly picked out of the parameter space, 19 421 did not violate current accelerator bounds. Of these, 825 result in relic densities of cosmological interest, i.e. $0.17 < \Omega_{DM} < 0.43$, the 95 per cent confidence interval quoted by Spergel et al. (2003). For sampling the MSSM parameter space we followed the choices of TO. For given telescope and observation parameters – i.e. the effective area A_{eff} , the integration time t , the angular resolution σ_θ , the radius of the field of view θ_{max} , the effective background count rate and the significance required for detection M_s – the smallest detectable cross-section $\langle\sigma v\rangle$ can be computed as a function of the neutralino mass m_χ (Bergström et al. 1998; Baltz et al. 2000, TO). In computing the expected signal, the volume of integration in equation (1) has to be taken as the volume of the halo contained within the chosen detection cell which will be the resolution element of the telescope for highly concentrated sources but may be much larger for diffuse sources such as the emission predicted in Fig. 7. We concentrate on estimating the γ -ray continuum signal which is easier to detect than the line signal (Baltz et al. 2000, TO).

Averaged over a gaussian beam of width $\sigma_\theta=0.1^\circ$, the resolution element for the telescopes listed in Table 1, the line-of-sight integral of the square of the mass density (equation A3) in the direction of the Galactic Centre takes values 5.2×10^{25} and 1.8×10^{24} $\text{GeV}^2 c^{-4} \text{cm}^{-5}$ for inward extrapolations of our NFW and SWTS fits to the main halo circular velocity curve. The large difference reflects the fact that this estimate is sensitive to density values far inside the region resolved by our simulations. Fig. 2 suggests that the lower value obtained from the SWTS extrapolation is more likely correct. To estimate the maximum plausible brightness for a subhalo, we examined the six artificial skies used to make Fig. 7 and identified the brightest subhalo in each after convolution with a 0.1° beam. The beam-averaged line-of-sight integral of density squared for the (apparently) brightest substructure in these six realisations is $4.9 \times 10^{23} \text{GeV}^2 c^{-4} \text{cm}^{-5}$.

To estimate detectability, we have to specify the appropriate background levels. We account for the electron-induced background in ACT observations, and for the extragalactic background emission in space-based observations. We neglect any hadronic background. All observations at low latitudes and in the general direction of the Galactic Centre are in addition affected by the diffuse Galactic γ -ray emission. Although this contribution can be neglected for ACT observations, it is the dominant background in these directions for space experiments like GLAST. In combination with the results of Fig. 7, this implies that the best signal-to-noise is expected for an observation of a broad broken annulus which *excludes* the Galactic Center and the Galactic Plane. If we assume that the diffuse galactic component drops to the level of the extragalactic background beyond 30° from the centre and 10° from the plane, a signal-to-noise ratio can be achieved which is about 12 times better than that for a 0.1° beam in the direction of the Galactic Centre (for an assumed NFW profile). This result is spectacular: the density profile of the DM halo in these regions is well established from the simulations and the prediction becomes *independen-*

Table 1. Simplified telescope specifications

	A_{eff} [m ²]	E_{th} [GeV c ⁻²]	σ_θ [°]	θ_{max} [°]
VERITAS	10 ⁴	50	0.1	1.75
GLAST	0.8	0.02	0.1	53

dent of numerical uncertainties in the innermost structure of CDM haloes.

These results are shown in Fig. 8. The solid curve gives our estimated lower limit on the cross-section for a $3\text{-}\sigma$ detection of the Galactic Centre in a 0.1° beam for a 250-h observation with the planned ACT VERITAS. This particular calculation extrapolates to small radii using the NFW model of Fig. 7 and the signal-to-noise is then maximised for the smallest resolved detection cell. The short-dashed curve is the corresponding limit for inward extrapolation using the SWTS model. In this case the signal-to-noise is maximised using a detection cell of radius 1.75° , corresponding to the full field of view of VERITAS. The corresponding lower limit for detection of the brightest substructure in our six artificial skies, again for a 1.75° beam, is shown by the long dashed curve. We assume the inner density structure of this object to be correctly described by our SWTS model fit. A 250-h observation may just be enough to detect the Galactic Centre, at least for a few of the plausible MSSM models. Detection of substructure appears out of reach unless our simulations have grossly underestimated the central concentration of subhaloes.

Fig. 8 also shows cross-section limits for a 1-yr exposure with the satellite telescope GLAST. The straight long-dashed line is the limit for detecting the brightest satellite, assuming this to be outside the region with strong diffuse Galactic emission and using a detection cell of radius 5° corresponding to the the peak signal-to-noise angle. The straight solid line gives the limit for detecting annihilation radiation in an annulus between 25° and 35° from the Galactic Centre but excluding the region within 10° of the Galactic Plane. We assume that the total diffuse Galactic emission in this region is zero. The results here are quite encouraging. The inner Galaxy should be detectable for most allowable MSSM parameters, while the brightest substructure is also detectable for many of them (for TO’s implicitly adopted prior on the MSSM parameter space).

Whereas the field of view of GLAST covers almost a fifth of the full sky, the smaller field of view of VERITAS allows observation of only one object at a time. In addition, ACTs can only operate about 6 h per night. For these reasons we consider exposure times of 1 yr for GLAST and 250 h for VERITAS to be large but feasible.

6 DISCUSSION

We have directly estimated the γ -ray emissivity of the halo of the Milky Way using high resolution simulations of its formation in a standard Λ CDM universe. A series of resimulations of the same DM halo at different mass resolution allows us to check explicitly for numerical convergence in our results. We find that the resolution limit of our largest simulation is almost an order of magnitude smaller than the half-light radius for the annihilation radiation, and that our estimates of the total flux are almost converged. We argue that the annihilation radiation from substructure within the Galactic halo is dominated by the most massive subhaloes, is concentrated in the outer halo, and is less in total than the radiation from the smooth

³ www.physto.se/~edjso/darksusy/

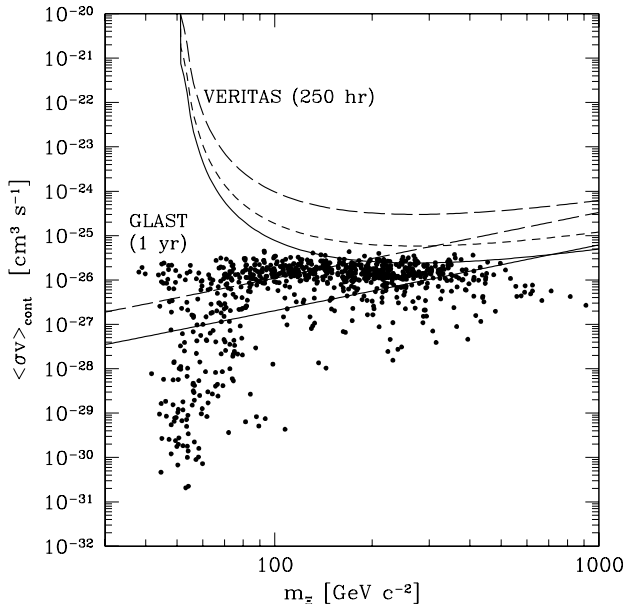


Figure 8. MSSM models of cosmological interest (dots) and $3\text{-}\sigma$ detection limits for VERITAS and GLAST. For VERITAS the limits are shown for a pointing at the centre of the Milky Way, assuming an NFW profile (solid) and an SWTS profile (short dashes). The lower solid line gives estimated limits for GLAST for a larger area observation of the inner Galaxy which avoids regions of high contamination by diffuse Galactic emission. Limits for a pointing at the brightest high latitude subhalo are shown for both telescopes using long dashes. The brightest subhalo was chosen from the 6 artificial skies used in making Fig. 7.

inner halo. For the most massive subhaloes our convergence study indicates sufficient resolution in our best simulations to get robust estimates of their internal structure. An important result is that subhalo cores are less concentrated both than that of the main halo and than those of their progenitor haloes. This confirms earlier results by SWTS and Hayashi et al (2003) and apparently reflects the influence of tidal shocking on subhalo structure.

We find that 15 per cent of the total flux in our highest-resolution simulation is coming from gravitationally bound subhaloes and that no more than about 5 per cent can be assigned to other small-scale density fluctuations. Some of our results do rely strongly on the density behaviour we infer from our simulations for the innermost regions both of the main halo and of the subhaloes. This subject is still controversial, although the most detailed convergence study to date agrees quite well with our results for the centre of the main halo (Power et al. 2003). As already noted, our subhalo structure agrees well with that found by Hayashi et al (2003). The disagreement between our results and other theoretical work on annihilation luminosities (Calcano-Rodan & Moore 2000, Tasitsiomi & Olinto 2002, Taylor & Silk 2003) can be traced to the fact that the density profiles adopted in these papers are incompatible with those we measure in our simulations, particularly for subhaloes. It may be relevant that observational data on dwarf galaxies also speak in favour of dark matter density profiles with low concentrations or cores (de Blok et al. 2001) although again the situation is controversial here.

To estimate the fluxes expected for deep integrations with upcoming experiments, it is necessary to extrapolate density profiles down to scales at least an order of magnitude below those where

they can be reliably estimated in our simulations. Clearly, this introduces substantial uncertainty. Our results suggest that the central regions of the Galaxy will be intrinsically more luminous than the brightest substructure by a factor of at least 10, and apparently more luminous by a factor approaching one thousand. The angular scale associated with the central emission will be several tens of degrees while that associated with the substructure will be a few degrees. This suggests that it may be worthwhile to investigate detection strategies which are sensitive to large-scale diffuse emission. Notice that since our results imply that the most apparently luminous subhaloes will also be among the most massive, it is likely that the brightest substructure source will be identified with one of the known satellites of the Milky Way. The closest of these is the Sagittarius dwarf at a distance of 24 kpc, but it may well be outshone by the LMC at a distance of 45 kpc. Both are sufficiently far that they will be much fainter (and smaller in angular size) than the main halo source which is centred only 8 kpc away.

Following TO, and using DARKSUSY, we checked for detectability of the inner Milky Way with VERITAS and GLAST, examples of ground- and space-based next-generation telescopes, respectively. If we extrapolate our simulated density profiles inwards using an NFW fit, VERITAS can probe into the parameter ranges in which a minimal supersymmetric extension of the Standard Model could provide a Dark Matter candidate with the observed cosmic density. Unfortunately, extrapolating inwards using our SWTS fit, which appears to provide a better description of our simulations, results in lower predicted fluxes, undetectable for VERITAS.

By searching for extended emission outside the central region where diffuse Galactic γ -ray emission is dominant GLAST can probe a large region of possible MSSM models. This result is based on the DM distribution in regions where the simulations have reliably converged, and so should be robust. It is *independent* of the exact structure of the DM in the innermost regions.

Our simulations suggest that the flux from the inner Galaxy will outshine the brightest substructure by a large factor. Nevertheless, for certain MSSM models some of the most massive substructure haloes might be detectable with GLAST. Clearly the most massive and nearest *known* satellite galaxies are the primary targets for observation.

ACKNOWLEDGMENTS

We thank Eric Nuss, Karsten Jedamzik, Argyro Tasitsiomi, Pasquale Blasi, Paolo Gondolo and Torsten Enßlin for many enlightening discussions.

REFERENCES

- Baltz E. A., Briot C., Salati C., Taillet R., Silk J., 2000, *Physical Review*, 61
- Bergström L., Edsjö J., Gondolo P., Ullio P., 1999, *Physical Review*, 59
- Bergström L., Ullio P., Buckley J. H., 1998, *Astroparticle Physics*, 9, 137
- Bullock J. S., Kolatt T. S., Sigad Y., et al., 2001, *MNRAS*, 321, 559
- Calcano-Roldán C., Moore B., 2000, *Physical Review*, 62
- de Blok W. J. G., McGaugh S. S., Rubin V. C., 2001, *AJ*, 122, 2396

- Dekel A., Arad I., Devor J., Birnboim Y., 2002, in astro-ph/0205448
- Font A. S., Navarro J. F., Stadel J., Quinn T., 2001, ApJL, 563, L1
- Hayashi E., Navarro J. F., Taylor J. E., Stadel J., Quinn T., 2003, ApJ, 584, 541
- Helmi A., White S. D., Springel V., 2002, Physical Review, 66, 63502
- Hernquist L., 1990, ApJ, 356, 359
- Klypin A., Kravtsov A. V., Valenzuela O., Prada F., 1999, ApJ, 52, 82
- Lake G., 1990, Nature, 346, 39+
- Metcalfe R. B., Madau P., 2001, ApJ, 563, 9
- Moore B., Ghigna S., Governato F., et al., 1999, ApJL, 524, L19
- Navarro J. F., Frenk C. S., White S. D. M., 1997, ApJ, 490, 493+
- Nusser A., Sheth R. K., 1999, MNRAS, 303, 685
- Peebles P. J. E., 1980, The Large-Scale Structure of the Universe, Princeton
- Power C., Navarro J. F., Jenkins A., et al., 2003, MNRAS, 338, 14
- Spergel D. N., Verde L., Peiris H. V., et al., 2003, ArXiv Astrophysics e-prints, 2209+
- Springel V., White S. D. M., Tormen G., Kauffmann G., 2001a, MNRAS, 328, 726
- Springel V., Yoshida N., White S. D. M., 2001b, New Astronomy, 6, 79
- Stoehr F., White S. D. M., Tormen G., Springel V., 2002, MNRAS, 335, L84
- Subramanian K., Cen R., Ostriker J. P., 2000, ApJ, 538, 528
- Syer D., White S. D. M., 1998, MNRAS, 293, 337+
- Tasitsiomi A., Olinto A. V., 2002, Physical Review, 66, 83006
- Taylor J. E., Silk J., 2003, MNRAS, 339, 505
- Tormen G., Bouchet F. R., White S. D. M., 1997, MNRAS, 286, 865
- Ullio P., Bergström L., Edsjö J., Lacey C., 2002, Physical Review, 66, 123502

APPENDIX A: DETECTABILITY COMPUTATION

We summarise briefly how the detectability lines of Fig. 8 were computed following Bergström et al. (1998), Baltz et al. (2000), Ullio et al. (2002) and TO. The solid angle corresponding to the angular resolution σ_θ of the telescope may be written as:

$$\Delta\Omega = 2\pi [1 - \cos(\sigma_\theta)], \quad (\text{A1})$$

while the number of continuum photons arriving on the telescope is

$$N_{\text{annihilation}} = A_{\text{eff}} t \frac{N_{\text{cont}}}{2} \frac{\langle\sigma v\rangle}{m_\chi^2} \frac{\Delta\Omega}{4\pi} G_{\text{los},\Delta\Omega}. \quad (\text{A2})$$

Here, $G_{\text{los},\Delta\Omega}$ stands for the line-of-sight integral of the DM distribution averaged over the solid angle $\Delta\Omega$:

$$G_{\text{los},\Delta\Omega} = \frac{1}{\Delta\Omega} \int_{\Delta\Omega} d\Omega \int_{\text{los}} \rho_{\text{DM}}^2(l) dl. \quad (\text{A3})$$

Values for $G_{\text{los},\Delta\Omega}$ are given in Section 5. TO give an approximate formula to compute the number continuum photons from one annihilation:

$$N_{\text{cont}}(E_\gamma > E_{th}) = \frac{5}{6}x^{3/2} - \frac{10}{3}x + 5x^{1/2} + \frac{5}{6}x^{-1/2} - \frac{10}{3} \quad (\text{A4})$$

Here $x = E_{th}/m_\chi$ is the quotient of the energy threshold of the telescope and the neutralino mass. Finally, the significance of a de-

tection M_s is given by the number of detected photons from DM annihilations over the square root of the background:

$$M_s \leq \frac{N_{\text{annihilation}}}{\sqrt{N_{\text{background}}}}. \quad (\text{A5})$$

This allows us to compute the minimal detectable cross-section $\langle\sigma v\rangle_{\text{min}}$ as a function of the mass of the neutralino m_χ via:

$$\langle\sigma v\rangle_{\text{min}} = \frac{2 M_s m_\chi^2 \sqrt{N_{\text{background}}}}{N_{\text{cont}} A_{\text{eff}} t \frac{\Delta\Omega}{4\pi} G_{\text{los},\Delta\Omega}} \quad (\text{A6})$$

The detectability scales with M_s , $t^{-1/2}$ and $A_{\text{eff}}^{-1/2}$. The background counts (hadronic, electron-induced, diffuse-galactic (for the centre of the galaxy) and extra-galactic) are taken from Bergström et al. (1998) and Baltz et al. (2000):

$$\frac{dN_h}{dt dA d\Omega} = 6.1 \times 10^{-3} \left(\frac{E_{th}}{1 \text{ GeV}/c^2} \right)^{-1.7} \text{ cm}^{-2} \text{ s}^{-1} \text{ sr}^{-1} \quad (\text{A7})$$

$$\frac{dN_e}{dt dA d\Omega} = 3.0 \times 10^{-2} \left(\frac{E_{th}}{1 \text{ GeV}/c^2} \right)^{-2.3} \text{ cm}^{-2} \text{ s}^{-1} \text{ sr}^{-1} \quad (\text{A8})$$

$$\frac{dN_d}{dt dA d\Omega} = 5.1 \times 10^{-5} \left(\frac{E_{th}}{1 \text{ GeV}/c^2} \right)^{-1.7} \text{ cm}^{-2} \text{ s}^{-1} \text{ sr}^{-1} \quad (\text{A9})$$

$$\frac{dN_{eg}}{dt dA d\Omega} = 1.2 \times 10^{-6} \left(\frac{E_{th}}{1 \text{ GeV}/c^2} \right)^{-1.1} \text{ cm}^{-2} \text{ s}^{-1} \text{ sr}^{-1} \quad (\text{A10})$$